



HAL
open science

Effect of spray drying treatment on the optical properties of Mg–Al spinel ceramics

Robin Stocky, Judith Boehmler, Sébastien Lemonnier, Pierre Gibot, Yannick Lorgouilloux, Anne Leriche

► **To cite this version:**

Robin Stocky, Judith Boehmler, Sébastien Lemonnier, Pierre Gibot, Yannick Lorgouilloux, et al.. Effect of spray drying treatment on the optical properties of Mg–Al spinel ceramics. Open Ceramics, 2021, 6, pp.100102. 10.1016/j.oceram.2021.100102 . hal-03365216

HAL Id: hal-03365216

<https://hal.science/hal-03365216>

Submitted on 6 Oct 2021

HAL is a multi-disciplinary open access archive for the deposit and dissemination of scientific research documents, whether they are published or not. The documents may come from teaching and research institutions in France or abroad, or from public or private research centers.

L'archive ouverte pluridisciplinaire **HAL**, est destinée au dépôt et à la diffusion de documents scientifiques de niveau recherche, publiés ou non, émanant des établissements d'enseignement et de recherche français ou étrangers, des laboratoires publics ou privés.

Effect of spray drying treatment on the optical properties of Mg-Al spinel ceramics

Robin Stocky^{a,c}, Judith Boehmler^{a,*}, Sébastien Lemonnier^a, Pierre Gibot^{a,b},
Yannick Lorgouilloux^c, Anne Leriche^c

^aInstitut Franco-Allemand de Recherches de Saint-Louis, 5 rue du Général Cassagnou, F-68301 Saint-Louis Cedex, France

^bLaboratoire des Nanomatériaux pour des Systèmes Sous Sollicitations Extrêmes (NS3E), ISL-CNRS-UNISTRA, UMR 3208, F-67081 Strasbourg, France

^cUniv. Polytechnique Hauts-de-France, EA 2443 - LMCPA - Laboratoire des Matériaux Céramiques et Procédés Associés, F-59313 Valenciennes, France

Abstract

One main challenge for transparent armour systems is to enhance the protection against specific threats and at the same time to reduce the weight. In recent years, Mg-Al spinel ceramic has been in the spotlight due to its advantages such as a large transparency range (UV, visible and mid-IR) and good mechanical properties. The aim of this work was to control the state of agglomeration of powder to improve the densification behaviour and consequently the optical and mechanical properties of the ceramics. Commercial powder with a small particle size was used and in the as-received conditions its poor flowability was found to be detrimental to its shaping and led to a translucent ceramic with an opaque rim. Therefore, the powder was granulated by spray drying and the influence of the molecular mass of added polyethylene glycol on the granulate size, compaction and finally sintering behaviour was investigated. Particular attention was paid to the difference in rheological behaviour between powders, which was carefully characterized with a FT4 powder rheometer. Sintering of powder with a controlled agglomeration ultimately resulted in transparent ceramics with an In-Line Transmission that reached 71% at $\lambda = 650$ nm, compared to 3% for ceramics obtained with the unmodified powder.

Keywords: Spinel, Transparent ceramics, Powder treatment, Spray drying, Powder rheology, Post-HIP

1. Introduction

Transparent magnesium aluminate spinel (MgAl_2O_4) ceramic combines good optical and mechanical properties making it a material of choice for missile domes, laser ignitors and ballistic transparent protection [1–4]. Magnesium aluminate spinel has a high melting point of 2135 °C, a high mechanical strength even at elevated temperatures, a high hardness of 16 GPa, a good chemical inertness and a low density, 3.58 g/cm³ [5, 6]. The high strength and wide transparency range (UV, visible and mid-IR) of spinel ceramic require a highly dense microstructure without pores, impurities, or secondary phases [7]. The residual porosity should be less than 0.01 vol% with a pore diameter below 100 nm to avoid scattering effect in the ceramic and to obtain a transparent spinel [7–9]. Indeed, porosity is highly detrimental to transparency as demonstrated by Benameur *et al.* who reported a reduction of In-Line Transmission (ILT) at 600 nm from 70% down to 10% as the porosity increased from 0.02% to 0.2% [10].

To completely eliminate porosity and obtain transparent spinel ceramics, it is generally necessary to use pressure-assisted sintering techniques such as Hot Pressing (HP) [22–25] or Spark Plasma Sintering (SPS) [9, 24–27], or to apply a post-treatment by Hot Isostatic Pressing (HIP) [8, 11–21]. Even if the sintering step is very important, all the different manufacturing process steps have to be thoroughly

controlled to obtain fully dense ceramics. Thereby shaping of the powder plays a crucial role and moreover, it is important to optimize the powder to obtain a homogeneous green body that leads to a highly transparent ceramic [8, 17, 18].

In order to obtain good mechanical properties, in particular high hardness, it is necessary to have a fine microstructure [43,44]. Indeed, a diminution of the grain size, below 10 μm , increases hardness following the Hall-Petch's law, as was successfully demonstrated on spinel ceramics by Krell *et al.* [43] and Sokol *et al.* [44]. Consequently, a fine and therefore reactive powder should ideally be selected to reach with the objective of developing fully dense ceramic with fine final grain size. Nonetheless, such very fine powders are known to be difficult to densify and in particular one of the main issues lies in their shaping into dense and homogeneous green bodies [8]. In general, the electrostatic behaviour of a fine ceramic powder limits its compaction by the formation of large and heterogeneous agglomerates [28]. An approach to remedy this situation and to obtain a good compaction could be to voluntarily agglomerate the powder in a controlled manner by granulation [29]. Esposito *et al.* used polyethylene glycol (PEG) with different molecular weights, between 200 and 600 g/mol, as a binder to granulate YAG nano powders into agglomerates of 2-10 μm . Granulation improved flowability, which allowed the preparation of uniform green bodies and resulted in a more homogeneous sintering [29]. Highly transparent ceramics were finally obtained with an increase of the ILT from 58% to 63% at 700 nm and of the final density from 4.58 g/cm³ to 4.76 g/cm³.

The purpose of the present work is to control the granulation of a very fine commercial spinel powder with the use of PEG as a binder to produce fine grain and fully dense ceramic. The impact of granulation on powder shaping and sintering behaviour is studied and its effect on the final microstructure and transparency quality is discussed.

2. Experimental

S25CRX MgAl₂O₄ spinel powder from Baikowski (France), especially designed for the study, exhibits an average particle size of 0.22 μm (d_{50}) and a specific surface area (S_{BET}) of 38 m²/g (supplier data). Phase composition was characterized by X-Ray diffraction (XRD) analysis, using a D8 Advance (Bruker) X-ray diffractometer from 10 to 100°2 θ with a time per step of 1 s and a step size of 0.009°2 θ . Crystalline phases were determined thanks to the EVA software. This powder will be named Reference hereafter.

Slurries containing 20wt.% of MgAl₂O₄ powder in absolute ethanol and 1wt.% polyethylene glycol (PEG) relatively to the mass of spinel powder, were prepared in a beaker with a magnetic stirrer. Three different molecular weights of PEG were considered: PEG 200, 400 and 600 (Rotipuran, Carl Roth). Granulation of the powder was done by using a Mini Spray Dryer B-290 (Buchi) equipped with an Inert Loop B295, under the following conditions: inlet temperature=120 °C, feed rate=15% and aspiration rate=90%.

The spray dried powders with PEG200, PEG400 and PEG600 are named in the following P200, P400 and P600, respectively. The rheological behaviour of Reference and granulated powders was studied by a FT4 powder rheometer (Freeman Technology) using 25 mL vessels and standard testing methods. The Stability Index (SI), Basic Flowability Energy (BFE), Specific Energy (SE), Permeability, Conditioned Bulk Density (CBD), Tapped Density (TD) and Compressed Density (CD) were determined.

The powder rheometer is equipped with a blade driven in a helical movement within the vessel containing the powder which is characterized. During this operation, the energy required to maintain a constant rotation speed was measured by recording the torque and the applied vertical force. Before each measurement, a conditioning step was conducted where the blade performed a down/up cycle at constant speed. This first step ensured better reproducibility of the measurements [31]. Each test was carried out at least three times with an identical powder mass, previously homogenized, in order to obtain good reproducibility of the measurements.

The Basic Flowability Energy (BFE) is measured by the energy required to establish a particular flow pattern in a conditioned volume of powder when the blade went down, and thereby to move the powder.

The Specific Energy (SE) was measured by the energy required to establish a particular flow pattern in a conditioned volume of powder when the blade went up.

The test necessary to measure BFE and SE was conducted 7 consecutive times. The Stability Index (SI) was calculated as the ratio of the energies required for the down displacement of the first and of the last cycle. A SI close to 1 corresponds to a stable powder.

The Permeability translates the ability of the powder to allow a flow of air to pass through it. It was

evaluated using a special base that allows to apply a flow of air through the powder bed from the bottom to the top at a constant speed of 2 mm/s. Increasing stresses were then applied by a piston to the powder bed and pressure drops across the powder bed were measured. For the comparison, the experiments were carried out with always the same starting volume of powder.

The densities CBD, TD and CD correspond to the densities of the powder in the different states. The CBD was calculated after the powder conditioning step (a preliminary down/up cycle of the blade at constant speed, as mentioned before) by simply dividing the powder mass by the apparent volume of the powder bed. The TD was measured the same way but after 50 tapping of the vessel containing the powder. The CD was measured after the application of a 15 kPa normal load.

Green bodies were prepared following a 2-steps process, i) uniaxial pressing under 50 MPa with an automatized universal press (5500-K9400, Instron) and ii) cold isostatic pressing (CIP) at 300 MPa (ACB). Organic binders were removed by a thermal treatment at 800 °C for 1 h in air [32] using a heating rate of 5 °C/min. Textural properties were determined by nitrogen (N₂) physisorption and mercury (Hg) intrusion. N₂ physisorptions at 77 K were carried out by means of an Accelerated Surface Area and Porosimetry system (ASAP 2020, Micromeritics, USA). Prior to the analyses, the samples were degassed at 250 °C under vacuum for 10 h. The specific surface areas (S_{BET}) were calculated according to the Brunauer-Emmett-Teller (BET) method within the 0.05–0.25 relative pressure range. Hg intrusion porosimetry technique (Autopore IV Micromeritics, USA) was used to determine the porosity of samples. Analyses were performed on pieces of broken samples to explore porosity in the core and on the surface of the samples. Assuming that the pores are cylindrical the applied pressure can be converted into the pore diameter by using the Washburn equation (1):

$$r = -2 \cdot \gamma \cdot \cos\theta / P \quad (1)$$

where P is the pressure required to force mercury into a pore of radius r, γ is the surface tension of mercury (485 dynes/cm) and θ is the contact angle (130°) between mercury and material.

Thereafter, samples were sintered in a high vacuum furnace (Lilliput, ECM Technology) for 2 h at 1350 °C and a heating rate of 10°C per minute. Based on the molecular weight of the PEG added to the powder, sintered ceramics are named in the following Sp200, Sp400 and Sp600, respectively and SpRef for the Reference powder. Sintered ceramics were then post-treated by hot isostatic pressing (HIP, EPSI Inc.) at 1450 °C under an argon pressure of 190 MPa, for 3 h with a heating rate of 3.3°C per min. These conditions of HIP were chosen according to the literature, with a temperature 100 °C above the sintering temperature [45].

HIP post-treated SpRef, Sp200, Sp400 and Sp600 ceramics will be named in the following study HRef, H200, H400 and H600 (Table 1). Finally, the dense ceramics were mirror-polished on both sides with an AutoMet300, (Buehler) by using polishing disks of 35 μ m, 15 μ m, 9 μ m and 3 μ m and finally a vibratory polisher with a diamond solution of 1 μ m vibratory polisher (VibroMet2, Buehler).

Densities were determined by hydrostatic weighing in distilled water calculating the average of values from three measurements for each of the three samples, according to the Archimedes method (EN 623- 2). Microstructures were observed on polished samples by scanning electron microscopy (SEM Nova NanoSEM 450, Thermo Fisher) using a Circular Backscatter Detector. The agglomerate and grain sizes were calculated by the average of 50 random measurements in four different observation areas with a total of 200 measurements (Feret diameter) by using ImageJ software (National Institutes of Health). The error was calculated by the standard deviation. In-Line Transmission was recorded from 300 nm to 3000 nm with an UV-VIS-IR spectrophotometer (Cary 7000 UMS, Agilent Technologies) and transmission results were normalized in respect to a final thickness of 2 mm [33].

3. Results and discussion

3.1. Reference spinel powder

XRD confirmed Mg-Al spinel (JCPDS 01-72-7232) as the major phase in the Reference MgAl₂O₄ powder (Figure 1 A), but the presence of MgO phase (JCPDS 01-089-7746) was also detectable. The MgO

percentage was determined by EVA software to approximately 4vol%. SEM observation (Figure 1 B) revealed non-spherical agglomerates which are composed of particles of 46 ± 12 nm. Calculation of the spherical particle size (D_{BET}) based on the specific surface area ($38 \text{ m}^2/\text{g}$) gives a diameter of 44 nm, which is thus consistent with our observations, by using the equation (2):

$$D_{\text{BET}} = (6.10^3) / (\rho \cdot S_{\text{BET}}) \quad (2)$$

Where ρ is absolute density of the spinel (3.58 g/cm^3) and S_{BET} is the specific surface area.

3.2. Compaction and sintering of the Reference powder

The green body relative density for the Reference powder was 48% and after sintering at $1350 \text{ }^\circ\text{C}$ density increased up to 95%. A white opaque ceramic was obtained after sintering, with an ILT at 650 nm close to zero.

The MgO phase could no longer be detected by XRD after the sintering step (not shown here). This indicates that MgO reacted with previously Mg-poor spinel during the sintering step, which led to stoichiometric spinel phase. An $\text{Al}_2\text{O}_3/\text{MgO}$ ratio of 0.98 was claimed by the powder supplier and ICP measures conducted during this study confirmed this value.

SEM observations of the Reference ceramic (SpRef) revealed a homogeneous microstructure and small average grain size of $0.8 \pm 0.3 \text{ }\mu\text{m}$. Nevertheless, the presence of numerous pores in the ceramic was observed, as shown in Figure 2 C.

HIP post-treatment led to a further increase of relative density, from 95% to 98%. The fine microstructure only slightly increased to $1.2 \pm 0.3 \text{ }\mu\text{m}$. As indicated by density measurements, intergranular porosity was still present in the ceramic shown in Figure 2 D. Regarding the optical aspect of the ceramic, the core became translucent, while the rim remained opaque (Figure 2A and B). This optical difference between rim and core was assigned to the amount of porosity, which was much higher in the rim part. This observation was confirmed by the SEM images in Figure 3, where the rim presents a higher level of porosity compared to the core of the sample. The origin of this phenomenon is explained in the literature by the presence of a stress gradient during uniaxial compaction [34–36]. This phenomenon is exacerbated when using powders with very small particle size. The visual aspect transcribes the poor compaction and rearrangement ability of the Reference powder.

3.3. Characterization of granulated powders

After spray drying, observations of the powders by SEM (Figure 4) revealed spherical agglomerates with sizes depending on the used PEG molecular weight. The agglomerate sizes of P200 and P400 powders were $12 \pm 2 \text{ }\mu\text{m}$ and $9.5 \pm 1.5 \text{ }\mu\text{m}$, respectively. P600 powder exhibited two types of agglomerate sizes: a larger one of $8.5 \pm 0.5 \text{ }\mu\text{m}$ and a smaller one of $3.8 \pm 0.9 \text{ }\mu\text{m}$. A decrease of the agglomerate size with the PEG molecular weight can be noticed. This observation is in agreement with the observation of Dobre *et al.* that the diameter of the agglomerates (D) after spray drying is inversely related to the viscosity of the suspension as shown by equation (3) where σ corresponds to the superficial tension of the spinel in the solvent (N/m), ρ to the density of the spinel (kg/m^3), μ to the dynamic viscosity of the slurry (kg/m.s), f the frequency of the spray dryer nozzle (Hz) and A a constant [37]. Here, the viscosity increases with the molecular weight of PEG.

$$D^5 = A \frac{\sigma^3}{\rho \mu^2 f^4} \quad (3)$$

The data of powder rheology measurements are summarized in Table 2. The stability, meaning that neither agglomeration nor attrition of the powder took place during manipulation, was evaluated. The low value (<1) of the stability index (SI) for the Reference powder displayed an unstable behaviour, tending to deagglomeration. The Reference powder is a very fine and electrostatic powder that forms soft agglomerates which were destroyed during the test. The processed powders P400 and P600 are stable (SI 1 ± 0.05) due to the spray drying and the binder that led to the formation of stronger agglomerates, which were conserved during stability test. P200 powder, being on the limit with a SI around 0.90, is considered as unstable. There are probably weak bonds between the powder particles inside the

agglomerates.

Next to the stability determination, Basic Flowability Energy (BFE) was found to reach a value of 108 mJ for the Reference, while for the three spray dried powders a lower BFE of around 50 mJ was measured. This difference can be attributed to the controlled agglomeration of the powder by spray drying. Indeed, the spherical shape of agglomerates after spray drying resulted in a decrease of friction and mechanical resistance within the powder bed and allowed a better sliding. In the Reference powder, as the agglomerates are of irregular shape (Figure 1b), the friction and mechanical resistance are stronger and thus more energy is needed to move the powder. Moreover, due to agglomeration the Reference powder is denser than the spray dried powder and hence more powder has to be moved. Focusing on the modified powders, small differences can also be highlighted. The powder spray dried with PEG600 exhibited a higher BFE value than the powders spray dried with PEG200 and 400. The higher BFE of the P600 powder value can be explained by a bimodal distribution of agglomerate size, while P200 and P400 powders show a mono-modal distribution of round-shaped agglomerates resulting in a better sliding behaviour [38]. Concerning the specific energy (SE), the Reference and the treated powders exhibited energies between 7 and 10 mJ/g, corresponding to a moderate cohesion. However, the SE of the Reference powder was slightly higher than that of the treated ones with ~10mJ/g compared to 7-8 mJ/g which indicates a better flowability of the spray dried powders.

The compaction behaviour of the various powders was studied by comparing the Conditioned Bulk Density (CBD) corresponding to the apparent density of powder, with the Tapped Density (TD), *i.e.* the density after mechanical tapping (50 times) and the Compressed Density (CD) measured after applying a 15 kPa normal stress on the powder. The results are summarized in Table 3.

The Reference powder had the highest bulk density (CBD) with 0.24 ± 0.01 g/mL. The processed powders had lower bulk densities with 0.19 ± 0.01 g/mL for P200, 0.21 ± 0.01 g/mL for P400 and 0.22 ± 0.01 g/mL for P600. The CBD values of the powders were relatively close to each other. The Reference powder had the highest bulk density, while P200 had the lowest. In addition, an increase of CBD was seen with increasing molecular weight of PEG, possibly due to the decrease in the size of the agglomerates, leading to a better arrangement of the powder. The Reference powder had also the highest TD with 0.30 ± 0.01 g/mL, while the treated powders had a TD of 0.26 ± 0.01 g/mL. However, this observation was reversed during compression under 15 kPa. Indeed, the density of the Reference powder only increased to 0.40 ± 0.01 g/mL during compression whereas the density of P200 and P400 powders reached a CD of 0.43 ± 0.01 g/mL and the one of P600 surpassed the other powders after compaction, with a CD of 0.44 ± 0.01 g/mL. This corresponds to a density increase of over 50% of spray dried powder compared to the Reference powder. A large porosity is supposed to have been present between the spherical agglomerates, which explains the loosely packed bulk powder bed resulting in the lower CBD. This was particularly visible for large agglomerates of P200 powder, which created larger porosity. Subsequently, the tapping allowed a rearrangement of the agglomerates, which led to an increase in density. However, there was always more porosity left in processed powders. On the contrary, under normal stress, the agglomerates of the spray dried powders underwent deformation, which reduced the size of the large inter-agglomerate pores and allowed to obtain denser compacts for the three modified powders [39].

Complementary to compression tests, the permeability of the powder was characterized. Indeed, a powder with a high compressed density (CD) should have a low permeability, as less porosity is present. The results are presented in Figure 5. The Reference powder had a higher permeability at 15 kPa (1.15 ± 0.01 cm²) compared to granulated powders with permeability values of 0.46 ± 0.03 cm² for P200, 0.54 ± 0.01 cm² for P400 and 0.55 ± 0.06 cm² for P600 powders. The lower permeability of modified powders showed a strong dependence between compression and reduction of air channels. The densities at 15 kPa (CD) were higher for granulated powders, the primary particles were therefore better organized and better compacted than in the Reference powder. This explains why air could be evacuated less easily and therefore the weaker permeability.

Powder characterization by FT4 powder rheometer allowed to illustrate the evolution of rheological behaviour and to highlight differences between the Reference powder and the spray dried powders. Granulated powders exhibit a better overall behaviour, which will be discussed in more details in the discussion section.

3.4. Green bodies of spray dried powders

A density of ~49% was determined for green bodies of spray dried powders, which is slightly higher than the density of the green body of Reference powder (48%). Specific surface areas of 35 m²/g were determined for all powders considered in this work. This result is consistent with the fact that powders consist of similar primary particles.

Regarding the Hg porosimetry analyses, an average pore size and a total pore volume of 29 ± 1 nm and 0.27 ± 0.01 mL/g, respectively, were determined for all green bodies, making it difficult even impossible to distinguish to each other (Figure 6). This total pore volume is in line with the apparent density of 49% calculated previously.

3.5. Sintering and HIP post-treatment of PEG-powders

After sintering, Sp200, Sp400 and Sp600 ceramics reached densities of 98%, 99% and 98%, respectively. In contrast, and as mentioned above, the SpRef exhibited a density of 95%.

All obtained ceramics showed a homogeneous microstructure and intergranular porosity (Figure 2 and Figure 7). Sp200 presented a grain size of 0.8 ± 0.3 µm, similar to SpRef. By increasing the PEG molecular weight, the grain size after sintering increased. For Sp400 a grain size of 1.6 ± 0.5 µm and for Sp600 a grain size of 2.8 ± 0.8 µm was determined. Moreover, the Sp200 ceramic revealed more pores than the Sp400 and Sp600 ceramics.

After HIP, the Reference ceramic showed a core/rim aspect (Figure 2), which was explained above by a porosity gradient within the ceramic, due to non-uniform compaction. For the H200 ceramic a transparent rim could be distinguished (Figure 8 A2) but the core of the ceramic had a cloudy aspect. In contrast, the rim totally disappeared for H400 and H600 and the transparency of both ceramics was found to be of higher quality (Figure 8 B2 and C2).

H200 ceramic reached a density of 99% while both H400 and H600 can be considered as fully dense. Nonetheless, despite the full or near full apparent densities of the ceramics, a low amount of residual pores was observed from SEM observations (Figure 9). SEM analyses also revealed homogeneous microstructures for the three HIPed processed ceramics with a slight increase of the average grain size compared to the Reference. Indeed, for the HRef, average grains size of 1.2 ± 0.3 µm was determined while values of 2.2 ± 0.6 µm, 3.5 ± 1.1 µm and 4.4 ± 1.6 µm were found for the H200, H400 and H600 samples, respectively.

ILT measurements were carried out and confirmed the previous optical observations. At λ = 650 nm, an ILT of 71% was reached for H600, 64% for H400, 21% for H200 and only 3% for the Reference ceramic (Figure 10). At 300 nm, the transmission values of Reference and H200 ceramics were close to zero, whereas an ILT of ~30% was measured for H400 and H600. Opacity of the Reference and H200 ceramics at 300nm indicates the presence of small pores, as pores have a higher impact on transparency at wavelengths close to the pore size [10, 16]. Between 1800- 3000 nm, all ceramics have an ILT over 70%, which is in agreement with the absence of very large pores confirmed by SEM (Figures 2 and 9).

3.6. Discussion

The powders were first compared based on their rheological behaviour. BFE and SE are directly linked to the physical properties of the powder such as particle size, distribution and shape, and therefore their specific surface areas. The four powders coming from the same starting powder, the primary particles are identical and thus if any differences in their behaviour can be identified, it will necessarily find its origin in the agglomeration state. The modified powders showed better flowability behaviours according to the BFE and less friction within the powder bed according to the SE (Figure 4). Granulated powders exhibit better compressibility with higher CD and this is confirmed by lower permeability.

The controlled agglomeration thus led to a better rearrangement of particles when a low load of 15 kPa was applied to the powders.

Densities obtained during rheology measurements and after cold isostatic pressing show clearly that it is difficult or even impossible to compare the compaction behaviour of the powder at

such very different applied pressures (15 kPa vs 300 MPa). From a macroscopic point of view, only the apparent density of the four samples are compared but from a microscopic point of view it is really difficult to conclude on the influence of rheology properties on the green bodies properties since characterizations of green bodies microstructure is complex. Indeed, pore size and distribution were expected to be much more homogeneous in the green body of spray dried powders than in the Reference powder [40, 47], but no clear differences could be highlighted at the green body stage. Nonetheless, an applied pressure of 15 kPa corresponds to the first instants of pressing and thus even if the rheological properties, different for Reference and spray dried powders, induce modifications in the compaction ability, the characterizations were carried out after an applied pressure higher for 3 orders of magnitude. Yet, a difference in the homogeneity and porosity distribution in the green body should be identified thanks to the optical aspects of the sintered ceramics. No difference in the characterization of the green bodies was observed, contrary to the final results. However, a difference in the porosity of the green bodies, between the core and the rim of the treated samples, cannot be totally excluded.

Nevertheless, the use of granulated powders clearly allowed to increase the density of the ceramics after the sintering step, from a density of 95% for the Reference to 98-99%. So, although no difference could be detected between green bodies prepared from treated or untreated powders, the spray-drying treatment clearly had an effect on the overall densification and the homogeneity of the ceramics. Granulated powders may be subject to an easier rearrangement during thermal treatments. This beneficial effect of rearrangement was also observed in other studies when lithium fluoride (LiF) was used as a sintering aid. Indeed, LiF leads to an improved sinterability, as it induces the formation of a liquid phase during densification, which is favourable to the rearrangement of particles [48-52]. This phenomenon takes place during early stage sintering [50], so liquid PEG may play a similar role at the very beginning of thermal treatment (during debinding treatment).

In addition, microstructures of all the materials were found to be different in terms of average grain size. It was already reported in the literature that the agglomeration state can influence grain growth during the sintering step [41, 42]. According to the authors, an increase of the agglomerate size is accompanied by a decrease of the shrinkage rate and finally an increase of grain growth is observed. This present study showed that the biggest agglomerates were obtained using the lowest PEG molecular weight, which led to a ceramic exhibiting smallest average grain size.

After post-HIP, the best results were obtained with PEG600 in terms of density and optical quality. The elimination of intergranular porosity in the ceramics after HIP post-treatment made it possible to obtain transparent (H400 and H600) or translucent (H200) ceramics (Figure 8). The use of granulation has shown an increase in grain size related to the molecular weight of PEG. So, the molecular weight of the binder clearly had an effect on the microstructure of sintered ceramics. It has to be noted that even if the grain size increased with the use of PEG, the grain size in all the final ceramics is still small compared to results published in the literature [11, 13, 19] with a grain size of less than 5 μm , for similar optical quality (normalized to the same thickness of 2 mm). Maca *et al.* proposed the sintering of a commercial spinel powder at 1500 °C and obtained a RIT of 60% (for a 1.1 mm thickness) with a grain size of 1 μm [11]. Although the grain size value is very attractive, the transmission is too low for transparent, ballistic protection application. Ramavath *et al.* succeeded in reaching an ILT value of 83% (normalized to a thickness of 2 mm) between 400 and 800 nm with sintering of the powder at 1650 °C [13]. However, these ceramics have an average grain size between 40 and 50 μm , which is beyond the limit value of 10 μm set in the literature with Hall-Petch's law [43,44]. Finally, Goldstein *et al.* presented a ceramic which has been sintered at 1480 °C with an ILT of 81% (normalized to a thickness of 2 mm also) between 400 and 800 nm and a grain size of 8 μm [19]. These results are more in agreement with a ballistic application, with an ILT greater than 70% and a grain size less than 10 μm .

The results presented in this study make the approach very promising from the grain size point of view considering the average value measured about 5 μm and the fact that the sintering parameters were fixed and not optimized. The developed ceramics exhibit grain size lower by a factor of 2 compared to Goldstein *et al.* [19] while their ILT is still compatible with the targeted

ballistic protection application. In addition, the heat treatment temperatures are lower than those used in the literature, with similar or even better results.

4. Conclusions

Transparent MgAl_2O_4 spinel ceramics were fabricated by uniaxial pressing, followed by CIP and densification by conventional sintering and post-HIP. Fine powder is generally reactive, but leads often to porosity and heterogeneous samples because shaping and processing can be challenging. Here, we demonstrated that the controlled agglomeration of a fine spinel powder is an easy method to significantly improve optical quality and obtain transparent ceramics with fine final average grain size. On the one hand, spray-drying with polyethylene glycol led to an improvement of the powder rheology behaviour. Nonetheless even if the improvement of the rheological behaviour makes the green body more homogeneous, the characterizations carried out did not allow to highlight any benefit of these improvements, probably due to the fact that characterizations were done after the application of a high uniaxial pressure compared to the pressure applied during rheological behaviour evaluation. On the other hand, the use of various molecular weights of PEG was studied and a clear influence of the molecular weight on optical quality of the final ceramic was illustrated. As the PEG molecular mass increased, the optical quality of samples improved to achieve high transparency for PEG600.

The spray drying treatment made it possible to improve the transparency of the ceramics and even the homogeneity of the ceramic, by reducing the core/rim aspect. These results are promising: the granulation made it possible to use very fine powders, which should allow to improve the transparency while limiting the final average grain size. Although differences, at the green body stage, could not be demonstrated by the characterizations of the samples, the final visual aspect of the different ceramics clearly indicates that spray drying, and thus rheological behaviour of the powder, strongly influenced the overall shaping process. Please notice that the starting powder used in the study was specifically developed and has not been the subject of other studies. A simple treatment on the Reference powder, which is very fine and very hard to shape, finally lead to a substantial improvement of the optical quality.

Further improvements of transparency and microstructures might be possible by optimizing HIP post-treatment conditions. This study is a first step towards the control of very fine powder to develop fully dense and fine gran size transparent ceramics which are expected to exhibit higher mechanical performances.

5. Acknowledgements

The authors would like to thank Thierry Bourré and Florence Moitrier for their contribution on sample preparation and SEM observations.

Funding

This work was supported by the French-German Research Institute of Saint-Louis, France.

References

- [1] J. L. Sepulveda, R. O. Loutfy, S. Chang, S. Ibrahim, N. Traggis, Advances in spinel ceramic technology for large windows and domes, in: *Window and Dome Technologies and Materials XI*, Vol. 7302, International Society for Optics and Photonics, 2009, p. 73020E.
- [2] J.-G. Li, T. Ikegami, J.-H. Lee, T. Mori, Fabrication of translucent magnesium aluminum spinel ceramics, *Journal of the American Ceramic Society* 83 (11) (2000) 2866–2868.
- [3] F. Tavangarian, R. Emadi, Synthesis and characterization of pure nanocrystalline magnesium aluminate spinel powder, *Journal of Alloys and Compounds* 489 (2) (2010) 600–604.
- [4] N. Stubièar, A. Tonejc, M. Stubièar, Microstructural evolution of some MgO-TiO_2 and $\text{MgO-Al}_2\text{O}_3$ powder mixtures

during high-energy ball milling and post-annealing studied by x-ray diffraction, *Journal of alloys and compounds* 370 (1-2) (2004) 296–301.

- [5] J.-G. Li, T. Ikegami, J.-H. Lee, T. Mori, Y. Yajima, A wetchemical process yielding reactive magnesium aluminate spinel (MgAl_2O_4) powder, *Ceramics International* 27 (4) (2001) 481–489.
- [6] N. Khalil, M. Hassan, E. Ewais, F. Saleh, Sintering, mechanical and refractory properties of ma spinel prepared via coprecipitation and sol-gel techniques, *Journal of Alloys and Compounds* 496 (1-2) (2010) 600–607.
- [7] M. Rubat du Merac, H.-J. Kleebe, M. M. Müller, I. E. Reimanis, Fifty years of research and development coming to fruition; unraveling the complex interactions during processing of transparent magnesium aluminate (MgAl_2O_4) spinel, *Journal of the American Ceramic Society* 96 (11) (2013) 3341–3365.
- [8] A. Krell, T. Hutzler, J. Klimke, A. Potthoff, Fine-grained transparent spinel windows by the processing of different nanopowders, *Journal of the American Ceramic Society* 93 (9) (2010) 2656–2666.
- [9] G. Bonnefont, G. Fantozzi, S. Trombert, L. Bonneau, Finegrained transparent MgAl_2O_4 spinel obtained by spark plasma sintering of commercially available nanopowders, *Ceramics International* 38 (1) (2012) 131–140.
- [10] N. Benameur, *Élaboration et caractérisations d'un spinelle polycristallin à grains fins transparent dans le visible et l'infrarouge*, Ph.D. thesis, Lille 1 (2009).
- [11] K. Maca, M. Trunec, R. Chmelik, Processing and properties of fine-grained transparent MgAl_2O_4 ceramics, *Ceramics Silikaty* 51 (2) (2007) 94.
- [12] T. J. Mroz, T. M. Hartnett, J. M. Wahl, L. M. Goldman, J. Kirsch, W. R. Lindberg, Recent advances in spinel optical ceramic, in: *Window and Dome Technologies and Materials IX*, Vol. 5786, International Society for Optics and Photonics, 2005, pp. 64–71.
- [13] P. Ramavath, P. Biswas, K. Rajeswari, M. B. Suresh, R. Johnson, G. Padmanabham, C. S. Kumbhar, T. K. Chongdar, N. M. Gokhale, Optical and mechanical properties of compaction and slip cast processed transparent polycrystalline spinel ceramics, *Ceramics International* 40 (4) (2014) 5575–5581.
- [14] K. Tsukuma, Transparent MgAl_2O_4 spinel ceramics produced by hip post-sintering, *Nippon Seramikkusu Kyokai Gakujutsu Ronbunshi* 114 (10) (2006) 802–806.
- [15] A. Witek, Preparing bulk transparent magnesium aluminium spinel—a few tricks of the trade, *Materiały Ceramiczne* 65 (3) (2013) 386–392.
- [16] A. Krell, K. Waetzig, J. Klimke, Influence of the structure of $\text{MgO} \cdot n\text{Al}_2\text{O}_3$ spinel lattices on transparent ceramics processing and properties, *Journal of the European Ceramic Society* 32 (11) (2012) 2887–2898.
- [17] A. Krell, J. Klimke, T. Hutzler, Advanced spinel and sub- μm Al_2O_3 for transparent armour applications, *Journal of the European Ceramic Society* 29 (2) (2009) 275–281.
- [18] A. Goldstein, A. Goldenberg, M. Hefetz, Transparent polycrystalline MgAl_2O_4 spinel with submicron grains, by low temperature sintering, *Journal of the Ceramic Society of Japan* 117 (1371) (2009) 1281–1283.
- [19] A. Goldstein, A. Shames, A. J. Stevenson, Z. Cohen, M. Vulfson, et al., Parasitic light absorption processes in transparent polycrystalline MgAl_2O_4 and YAG, *Journal of the American Ceramic Society* 96 (11) (2013) 3523–3529.
- [20] A. Krell, T. Hutzler, J. Klimke, Defect strategies for an improved optical quality of transparent ceramics, *Optical Materials* 38 (2014) 61–74.
- [21] C. Gajdowski, J. Böhmler, Y. Lorgouilloux, S. Lemonnier, S. d'Astorg, E. Barraud, A. Leriche, Influence of post-hip temperature on microstructural and optical properties of pure MgAl_2O_4 spinel: From opaque to transparent ceramics, *Journal of the European Ceramic Society* 37 (16) (2017) 5347–5351.
- [22] L. Esposito, A. Piancastelli, P. Miceli, S. Martelli, A thermodynamic approach to obtaining transparent spinel (MgAl_2O_4) by hot pressing, *Journal of the European Ceramic Society* 35 (2) (2015) 651–661.
- [23] L. Esposito, A. Piancastelli, S. Martelli, Production and characterization of transparent MgAl_2O_4 prepared by hot pressing, *Journal of the European Ceramic Society* 33 (4) (2013) 737–747.
- [24] M. Suárez, A. Fernández, R. Torrecillas, J. L. Menéndez, Sintering to transparency of polycrystalline ceramic materials, in: *Sintering of Ceramics-New Emerging Techniques*, InTech, 2012.
- [25] M. Suarez, V. Rocha, A. Fernández, J. Menéndez, R. Torrecillas, Synthesis and processing of spinel powders for transparent ceramics, *Ceramics International* 40 (3) (2014) 4065–4069.
- [26] K. Morita, B.-N. Kim, K. Hiraga, H. Yoshida, Fabrication of transparent MgAl_2O_4 spinel polycrystal by spark plasma sintering processing, *Scripta Materialia* 58 (12) (2008) 1114–1117.
- [27] K. Morita, B.-N. Kim, H. Yoshida, H. Zhang, K. Hiraga, Y. Sakka, Effect of loading schedule on densification of MgAl_2O_4 spinel during spark plasma sintering (sps) processing, *Journal of the European Ceramic Society* 32 (10) (2012) 2303–2309.
- [28] B. P. Saha, V. Kumar, S. Joshi, A. Balakrishnan, C. L. Martin, Investigation of compaction behavior of alumina nano powder, *Powder technology* 224 (2012) 90–95.
- [29] L. Esposito, A. Piancastelli, Role of powder properties and shaping techniques on the formation of pore-free YAG materials, *Journal of the European Ceramic Society* 29 (2) (2009) 317–322.
- [30] L. Esposito, A. L. Costa, V. Medri, Reactive sintering of YAGbased materials using micrometer-sized powders, *Journal of the European Ceramic Society* 28 (5) (2008) 1065–1071.
- [31] F. Technology, Powder testing, <https://www.tech.co.uk/> (2014). URL <https://www.freemantech.co.uk/>
- [32] T. Spusta, J. Svoboda, K. Maca, Study of pore closure during pressure-less sintering of advanced oxide ceramics, *Acta Materialia* 115 (2016) 347–353.
- [33] R. Apetz, M. P. Van Bruggen, Transparent alumina: a lightscattering model, *Journal of the American Ceramic Society* 86 (3) (2003) 480–486.
- [34] B. Lanfant, *Élaboration et étude des propriétés thermomécaniques de composites à matrice SiC nanostructurée renforcée par des nanotubes de carbone*, Ph.D. thesis, Université Paris Sud-Paris XI (2014).
- [35] C. Wang, Z. Zhao, Transparent MgAl_2O_4 ceramic produced by spark plasma sintering, *Scripta Materialia* 61 (2) (2009) 193–196.
- [36] A. Katz, *Élaboration de céramiques polycristallines transparentes Er^{3+} : YAG par spark plasma sintering pour applications laser de puissance*, Ph.D. thesis, Valenciennes (2016).
- [37] M. Dobré, *Caractérisation stochastique des sprays ultrasoniques: le formalisme de l'entropie maximale*, Ph.D. thesis,

Universite de LouvainBelgique (2003).

- [38] V. P. Onbattuvelli, R. K. Enneti, S.-J. Park, S. V. Atre, The effects of nanoparticle addition on sic and aln powder–polymer mixtures: Packing and flow behavior, *International Journal of refractory metals and hard materials* 36 (2013) 183–190.
- [39] B. P. Raghupathy, J. G. Binner, Spray granulation of nanometric zirconia particles, *Journal of the American Ceramic Society* 94 (1) (2011) 42–48.
- [40] L. Esposito, A. Piancastelli, A. L. Costa, M. Serantoni, G. Toci, M. Vannini, Experimental features affecting the transparency of YAG ceramics, *Optical Materials* 33 (5) (2011) 713–721.
- [41] J. Halloran, Role of powder agglomerates in ceramic processing, *Forming of Ceramics. Advances in Ceramics*. 9 (1983) 67.
- [42] M. A. Occhionero, J. Halloran, The influence of green density upon sintering, in: *Materials Science Research*, Springer, 1984, pp. 89–102.
- [43] Krell, A., & Bales, A. (2011). Grain size-dependent hardness of transparent magnesium aluminate spinel. *International Journal of Applied Ceramic Technology*, 8(5), 1108-1114.
- [44] Sokol, M., Halabi, M., Kalabukhov, S., & Frage, N. (2017). Nano-structured MgAl₂O₄ spinel consolidated by high pressure spark plasma sintering (HPSPS). *Journal of the European Ceramic Society*, 37(2), 755-762.
- [45] A. Goldstein, A. Goldenberg, M. Vulfson, Development of a technology for the obtained of fine grain size, transparent MgAl₂O₄ spinel parts, *Journal of the Ceramic Science and Technology* (2) (2011) 1–8.
- [46] Sarkar, R., Tripathi, H. S., & Ghosh, A. (2004). Reaction sintering of different spinel compositions in the presence of Y₂O₃. *Materials Letters*, 58(16), 2186-2191.
- [47] Lee, H. W., Song, G., & Suk, I. S. (1995). Effect of suspension property on granule morphology and compaction behavior (No. CONF-940416-). American Ceramic Society, Westerville, OH (United States).
- [48] Villalobos, G. R., Sanghera, J. S., & Aggarwal, I. D. (2005). Degradation of magnesium aluminum spinel by lithium fluoride sintering aid. *Journal of the American Ceramic Society*, 88(5), 1321-1322.
- [49] Rozenburg, K., Reimanis, I. E., Kleebe, H. J., & Cook, R. L. (2007). Chemical interaction between LiF and MgAl₂O₄ spinel during sintering. *Journal of the American Ceramic Society*, 90(7), 2038-2042.
- [50] Reimanis, I., & Kleebe, H. J. (2009). A review on the sintering and microstructure development of transparent spinel (MgAl₂O₄). *Journal of the American Ceramic Society*, 92(7), 1472-1480.
- [51] Sutorik, A. C., Gilde, G., Cooper, C., Wright, J., & Hilton, C. (2012). The effect of varied amounts of LiF sintering aid on the transparency of alumina rich spinel ceramic with the composition MgO· 1.5 Al₂O₃. *Journal of the American Ceramic Society*, 95(6), 1807-1810.
- [52] Müller, M. M., & Kleebe, H. J. (2012). Sintering mechanisms of LiF-doped Mg–Al-spinel. *Journal of the American Ceramic Society*, 95(10), 3022-3024.

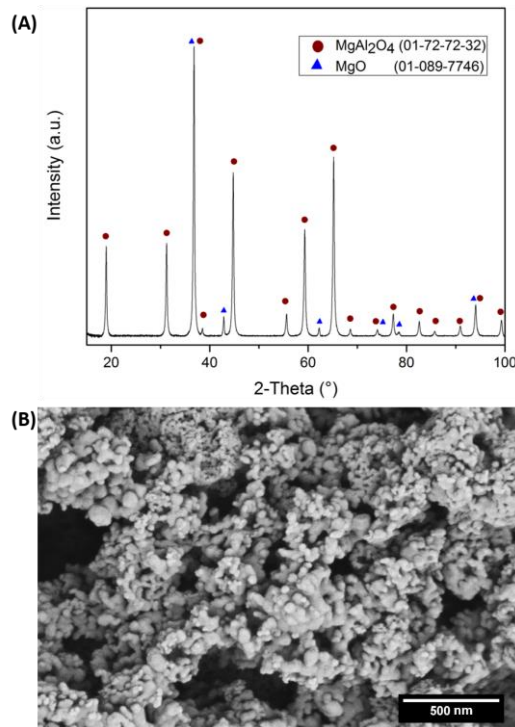


Figure 1: XRD patten (A) and SEM picture (B) of the Reference spinel MgAl₂O₄ powder.

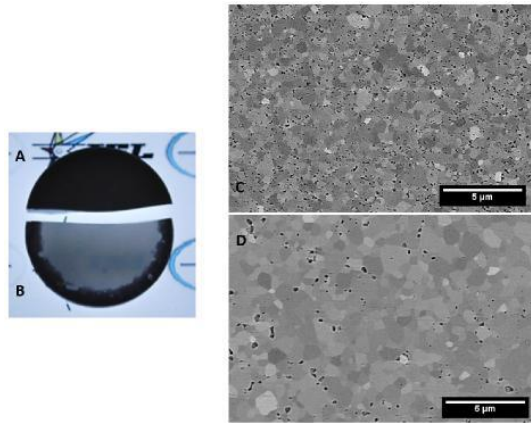


Figure 2: Observations on light table and by SEM of the Reference spinel powder after sintering SRef (A and C) and Reference spinel powder after post-HIP HRef (B and D)

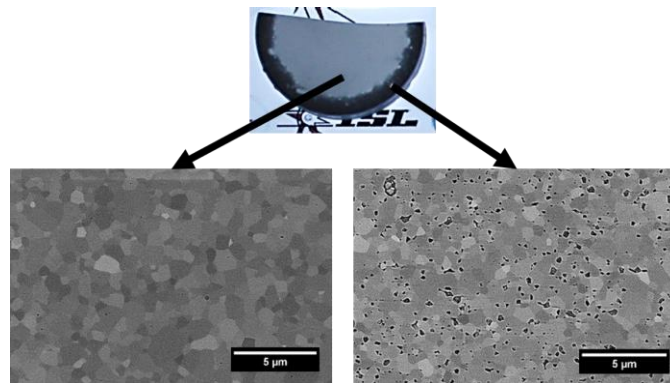


Figure 3 : SEM pictures of the core and rim of the Reference spinel $MgAl_2O_4$ powder after HIP

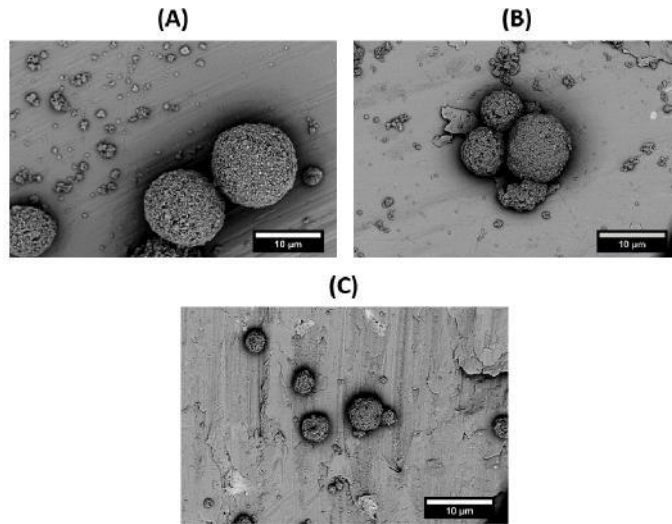


Figure 4: SEM pictures of the spray dried powders P200 (A), P400 (B) and P600 (C)

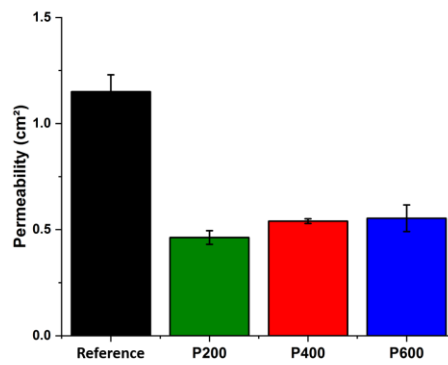


Figure 5 : Permeability at 15kPa of Reference spinel powder, spray dried powder with PEG200 (P200), spray dried powder with PEG400 (P400) and spray dried powder with PEG600 (P600)

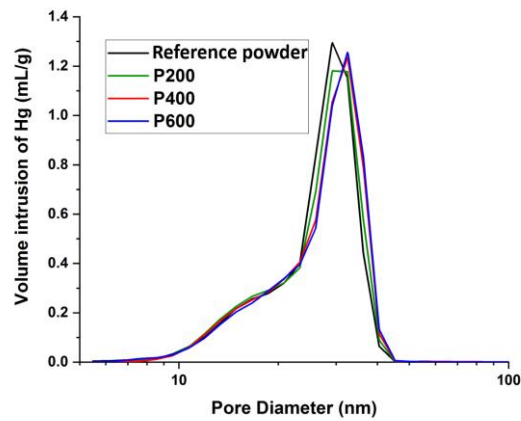


Figure 6 Pore size distributions of green bodies of Reference powder, P200, P400 and P600 green bodies determined by Hg porosimetry intrusion method

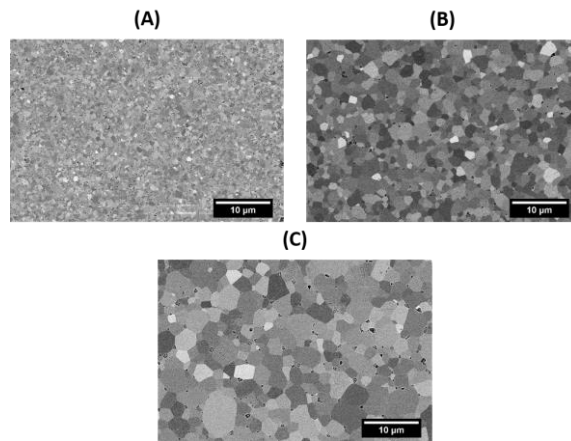


Figure 7: SEM pictures of sintered spinel samples (A) spray dried powder with PEG200 (P200), (B) spray dried powder with PEG400 (P400) and (C) spray dried powder with PEG600 (P600)

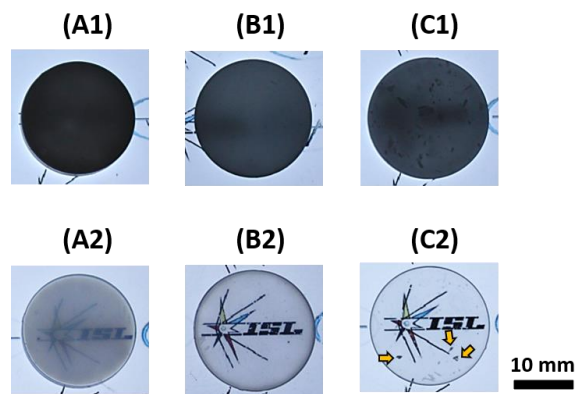


Figure 8: Pictures on light table of (top) sintered ceramics obtained with spray dried powders prepared with PEG200 (Sp200, A1), PEG400 (Sp400, B1) and PEG600 (Sp600, C1) and (bottom) HIPed ceramics obtained with spray dried powders prepared with PEG200 (H200, A2), PEG400 (H400, B2) and PEG600 (H600, C2). Defects are indicated by yellow arrows

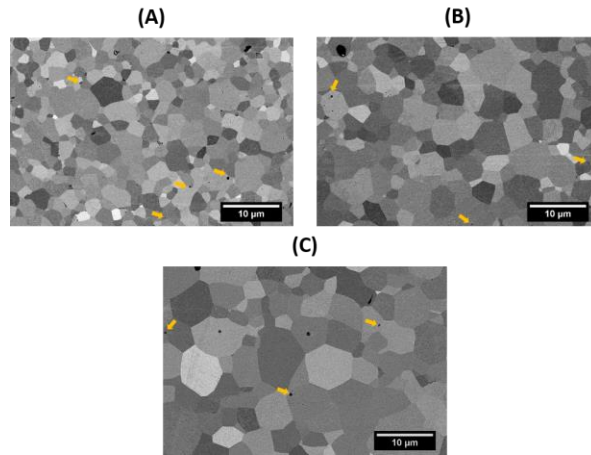


Figure 9 SEM pictures of HIPed spinel samples obtained with (A) spray dried powder prepared with PEG200 (H200), (B) PEG400 (H400) and (C) PEG600 (H600). Pores are indicated by yellow arrows

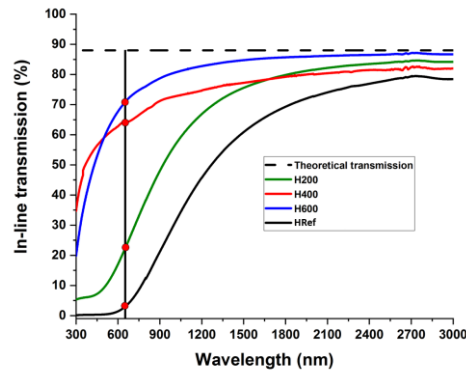


Figure 10: In-line transmission after HIP post-treatment (values normalized to a sample thickness of 2mm)

Powder	After Sintering	After HIP
Reference	SpRef	HRef
P200	Sp200	H200
P400	Sp400	H400
P600	Sp600	H600

Table 1: Notation of Reference powder and treated powders obtained by spray drying with PEG200, PEG400 and PEG600 at different stages (P:powder; Sp:sintered; H:HIPed)

	SI	BFE (mJ)	SE (mJ/g)
Reference	0.85 ± 0.04	108 ± 3	9.56 ± 0.38
P200	0.90 ± 0.05	48 ± 5	7.65 ± 0.45
P400	1.06 ± 0.05	40 ± 3	7.22 ± 0.41
P600	0.95 ± 0.06	58 ± 3	8.36 ± 0.29

Table 2: Rheological data of Reference, P200, P400 and P600 powders

	CBD (g/mL)	TD (g/mL)	CD (g/mL)
Reference	0.24 ± 0.01	0.30 ± 0.01	0.40 ± 0.01
P200	0.19 ± 0.01	0.26 ± 0.01	0.43 ± 0.01
P400	0.21 ± 0.01	0.26 ± 0.01	0.43 ± 0.01
P600	0.22 ± 0.01	0.26 ± 0.01	0.44 ± 0.01

Table 3: Densities of Reference, P200, P400 and P600 powders